Design of surface emitting distributed feedback quantum cascade laser with single-lobe far-field pattern and high outcoupling efficiency*

Guo Wan-Hong(郭万红)†, Liu Jun-Qi(刘俊岐)‡, Lu Quan-Yong(陆全勇), Zhang Wei(张 伟), Li Lu(李 路), Wang Li-Jun(王利军), Liu Feng-Qi(刘峰奇), and Wang Zhan-Guo(王占国)

Key Laboratory of Semiconductor Materials Science, Institute of Semiconductors, Chinese Academy of Sciences, Beijing 100083, *China*

(Received 9 October 2009; revised manuscript received 21 October 2009)

A 7.8-μm surface emitting second-order distributed feedback quantum cascade laser (DFB QCL) structure with metallized surface grating is studied. The modal property of this structure is described by utilizing coupled-mode theory where the coupling coefficients are derived from exact Floquet–Bloch solutions of infinite periodic structure. Based on this theory, the influence of waveguide structure and grating topography as well as device length on the laser performance is numerically investigated. The optimized surface emitting second-order DFB QCL structure design exhibits a high surface outcoupling efficiency of 22% and a low threshold gain of 10 cm^{-1}. Using a π phase-shift in the centre of the grating, a high-quality single-lobe far-field radiation pattern is obtained.

Keywords: quantum cascade laser, Floquet–Bloch expansion, distributed feedback lasers, surface emission

PACC: 4255P, 4280F, 6120J

1. Introduction

The quantum cascade laser (QCL) is a compact and powerful semiconductor light source in mid- and far-infrared wavelength ranges.[1,2] For the practical applications such as chemical sensing and pollution monitoring,[3] the single-mode emission is highly required, which can be easily realized by first-order distributed feedback (DFB) edge-emitting QCLs. On the other hand, the surface emission is also widely fascinating since it would greatly facilitate two-dimensional integration and on-wafer testing. Nevertheless, the conventional vertical cavity surface-emitting lasers[4−7] are not feasible for transverse magnetic (TM) polarized QCLs. To achieve surface emission, second-order DFB gratings[8−11] or photonic crystal (PhC) resonators[12] are usually incorporated into the QCLs. However, the fabrication of PhC lattice is challenging since it requires a deep etching technique with a high aspect ratio and a precise control of the air filling factor. Thus, the second-order DFB grating etched just into the upper waveguide layers is preferable to realize QCLs with both single-mode and surface emission.

Although surface-emitting DFB QCLs have been experimentally realized by several groups,[8−11] recently, there is still much room to improve the surface outcoupling efficiency and far-field distribution by the design of waveguide structure and grating topography. In this paper, a numerical investigation of the waveguide structure, the grating height as well as the grating duty cycle, and the device length of a surface-emitting DFB QCL is carried out by using a coupled-mode theory. This theory is derived from rigorously computed on-resonant Floquet–Bloch solutions of the waveguide-grating problem and hence enables the accurate simulating of second-order gratings with large grating heights or strong index contrasts. An optimal 7.8 μm surface emitting second-order DFB QCL structure is proposed, which shows a high surface outcoupling efficiency of 22% and a low threshold gain of 1 cm^{-1}. High-quality single-lobe far-field radiation

*Project supported by the National Science Fund for Distinguished Young Scholars of China (Grant No. 60525406), the National Natural Science Foundation of China (Grant Nos. 60736031, 60806018, and 60906026), the National Basic Research Program of China (Grant No. 2006CB604903), and the National High Technology Research and Development Program of China (Grant Nos. 2007AA03Z446 and 2009AA03Z403).

†Corresponding author. E-mail: whguo@semi.ac.cn

‡E-mail: jqliu@semi.ac.cn

© 2010 Chinese Physical Society and IOP Publishing Ltd

pattern is also obtained by adding a π phase-shift in the centre of the grating.

2. Theory

2.1. Floquet–Bloch solutions for the infinite-length laser structure

The analysis of surface-emitting lasers expresses the modes of a finite length laser as linear combinations of the exact eigenmodes of an infinite length laser. We consider only TM-polarized modes where the magnetic field is in the y-axis direction as shown in Fig. 1. Because of the periodic nature of the laser structure in the z-axis direction, the magnetic field can be written exactly as a Floquet–Bloch expansion

$$H(x,z) = \sum_{m=0,\pm1,\cdots} H_m(x)\,\mathrm{e}^{\mathrm{i}\,\beta_m z}, \tag{1a}$$

where

$$\beta_m = \beta_0 + mK. \tag{1b}$$

Here, β_0 is the complex-valued propagation constant and $\boldsymbol{K} = 2\pi/\Lambda$ denotes the grating vector. In this expression, H_{-1} describes the surface emission field. The partial waves H_m $(m = 0, \pm1, \ldots)$ satisfy the following complex eigenvalue equations[13]

$$\frac{\mathrm{d}^2 H_m}{\mathrm{d}x^2} = \sum_p \left\| \frac{1}{\varepsilon} \right\|^{-1}_{\mathrm{mp}} \sum_q \left(\beta_p \left\| \varepsilon \right\|^{-1}_{pq} \beta_q - k_0^2 \delta_{pq} \right) H_q, \tag{2}$$

where $||f||$ denotes the Toeplitz matrix generated by the Fourier coefficients of f such that its (p,q) entry is f_{p-q}, δ_{pq} is the Kronecker symbol, -1 denotes the matrix inverse, and k_0 is the free-space propagation constant. Equations (2) are solved under the continuity conditions[14] and the outgoing radiation boundary conditions.[15] For the sake of simplicity, we truncate the infinite set of Floquet–Bloch expansion partial waves to the finite set including the orders from $m = -8$ to 8, which results in estimated relative errors of less than 10^{-3} for the real part of β and less than 4% for the imaginary part of β, respectively.

2.2. Coupled-mode theory for the finite-length laser structure

To compute the threshold gain and the surface outcoupling efficiency, a pair of coupled-wave equations is deduced for the second-order DFB QCLs and written as

$$\begin{aligned} &\frac{\mathrm{d}S}{\mathrm{d}z} + \left(-\mathrm{i}\,\varsigma - G - \frac{\mathrm{i}\,\delta}{2} \right) S = \mathrm{i}\,\kappa R, \\ &-\frac{\mathrm{d}R}{\mathrm{d}z} + \left(-\mathrm{i}\,\varsigma - G - \frac{\mathrm{i}\,\delta}{2} \right) R = \mathrm{i}\,\kappa S. \end{aligned} \tag{3}$$

Here, R and S represent the z-dependent amplitudes of the forward wave and the backward wave, respectively, G is the field gain coefficient at threshold, and δ denotes the normalized frequency. The expressions of the self-coupling coefficient ζ and the mutual coupling coefficient κ can be found in Ref. [14].

Once ζ, κ and the device length L are given, the field threshold gain coefficient G and associated parameter δ as well as the amplitudes $R(z)$ and $S(z)$ can be obtained by solving the above coupled-wave equations. Finally, the actual threshold power gain coefficient is given by[16]

$$g_{\mathrm{th}} = 2G. \tag{4}$$

The surface emitting magnetic field is obtained to be

$$H^{(\mathrm{surface})}(z) = R(z) + S(z). \tag{5}$$

The surface outcoupling efficiency is written as[17]

$$\eta_{\mathrm{surf}} = \frac{k_0}{K} \frac{n_{\mathrm{act}}}{\Gamma g_0} \alpha_{\mathrm{surf}} \frac{\int \mathrm{d}z\,|R(z)+S(z)|^2}{\int \mathrm{d}z(|R(z)|^2 + |S(z)|^2)}, \tag{6}$$

where n_{act} is the refractive index of the active layer, α_{surf} is the surface loss, Γ is the active layer confinement factor, and g_0 is the gain coefficient in the active region.

3. Device optimization

3.1. Waveguide design

It is a key issue for surface-emitting DFB QCLs[8−11] to improve the surface-emitting efficiency with still maintaining an acceptable level of threshold gain. To solve this problem it is necessary to design a proper waveguide first. In this paper, we optimize a waveguide structure on the basis of one similar to that in Ref. [18] as shown in Fig. 1. To obtain a wide gain spectrum, the active region is adopted to be identical to that in Ref. [19]. The effect of the thickness of every waveguide layer on the device performance is numerically investigated.

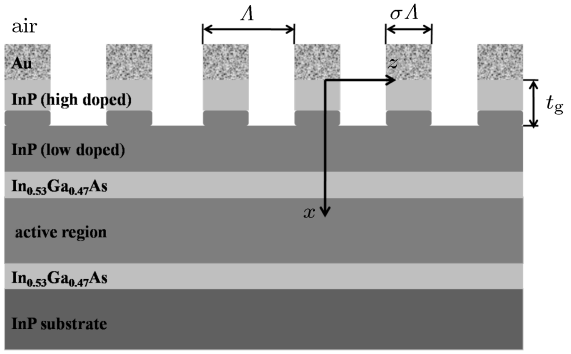


Fig. 1. Schematic cross section of the second-order DFB QCL structure, where the grating has periodicity Λ, duty cycle σ and grating height $t_{\rm g}$.

The complex refractive indexes of the layers constituting the QCL are $n_{\rm active_region} = 3.335 + {\rm i}*1 \times 10^{-4}$ (Si, 8×10^{16} cm^{-3}), $n_{\rm InP_substrate} = 3.066 + {\rm i}*1 \times 10^{3}$ (Si, 3×10^{17} cm^{-3}), $n_{\rm InP_high-doped} = 2.257 + {\rm i}*0.0708$ (Si, 7×10^{18} cm^{-3}), $n_{\rm InP_low-doped} = 3.0886 + {\rm i}*3 \times 10^{-4}$ (Si, 1×10^{17} cm^{-3}), $n_{\rm InGaAs} = 3.4005 + {\rm i}*2 \times 10^{-4}$ (Si, 6×10^{16} cm^{-3}), and $n_{\rm Au} = 7.78 + {\rm i}*57$. These values are obtained from a Drude–Lorentz model[20]

$$(n - {\rm i}\,k)^2 = \varepsilon_\infty \left[1 - \frac{\omega_{\rm p}^2}{\omega^2 \eta}\left(1 + \frac{\rm i}{\omega\tau}\right)\right], \qquad (7)$$

where n and k are the real and the imaginary parts of the refractive index; τ is the electron scattering time evaluated by the electron mobility $\mu_{\rm e}$ and the effective electron mass $m_{\rm e}$ as $\tau = \mu_{\rm e} m_{\rm e}/e$ and $\eta = 1 + 1/(\omega\tau)^2$; $\omega_{\rm p}$ is the plasma frequency, given by $\omega_{\rm p}^2 = Ne^2/m_{\rm e}\varepsilon_\infty\varepsilon$, where N is the concentration and ε_∞ is the high-frequency lattice dielectric constant. For the wavelength of 7.8 μm, the values of $\mu_{\rm e} m_{\rm e}$ and ε_∞ at room temperature are obtained according to Refs. [21]–[23], and listed in Table 1. The refractive index of Au is cited from Ref. [24].

Table 1. Values of $\mu_{\rm e}$, $m_{\rm e}$ and ε_∞ obtained at 7.8 μm wavelength and room temperature.

material	doping/cm^{-3}	$\mu_{\rm e}$/(cm^2·V^{-1}·s^{-1})	$m_{\rm e}/m_0$	ε_∞
InP	1×10^{17}	34487	0.0774	9.61
InP	3×10^{17}	28827	0.0778	9.61
InP	7×10^{18}	12276	0.0839	9.61
InGaAs	6×10^{16}	10286	0.0412	11.642
InGaAs	8×10^{16}	8097	0.0415	11.642
InAlAs	8×10^{16}	841	0.075	10.313

By varying the thickness of each waveguide layer, we find that only the high-doped InP layer (contact layer) has a significant influence on the surface outcoupling efficiency $\eta_{\rm surf}$ and the threshold gain $g_{\rm th}$. Now the thicknesses of the waveguide layers except the top contact are fixed to be as follows: $t_{\rm active_region} = 2.296$ μm, $t_{\rm InP_low-doped} = 2$ μm, $t_{\rm InGaAs} = 0.25$ μm and $t_{\rm Au} = 0.4$ μm. The values of $\eta_{\rm surf}$ and $g_{\rm th}$, each as a function of the contact layer thickness, are plotted in Fig. 2(a). In the calculation, the grating height $t_{\rm g}$ and the duty cycle σ are experientially fixed to be 1 μm and 0.6, respectively. For efficient surface emission, $|\kappa L|$ must be around 1–2, where the optical intensity is more or less uniformly distributed throughout the device according to the demonstration in Ref.[14]. Additional simulation results reveal that the exact value of $|\kappa L|$, in a range of 1–2, has little influence on the optimal waveguide and grating design. Thus without losing generality, $|\kappa L| = 1$ is used here and also in the latter calculations. As shown in Fig. 2(a), $\eta_{\rm surf}$ and $g_{\rm th}$ both increase monotonically with the decrease of the thickness of contact layer. This can be explained by the simultaneous increase of surface loss which represents a fraction of surface emission light while the absorption loss and substrate loss experience little changes with the minishing of the contact layer thickness as shown in Fig. 2(b).

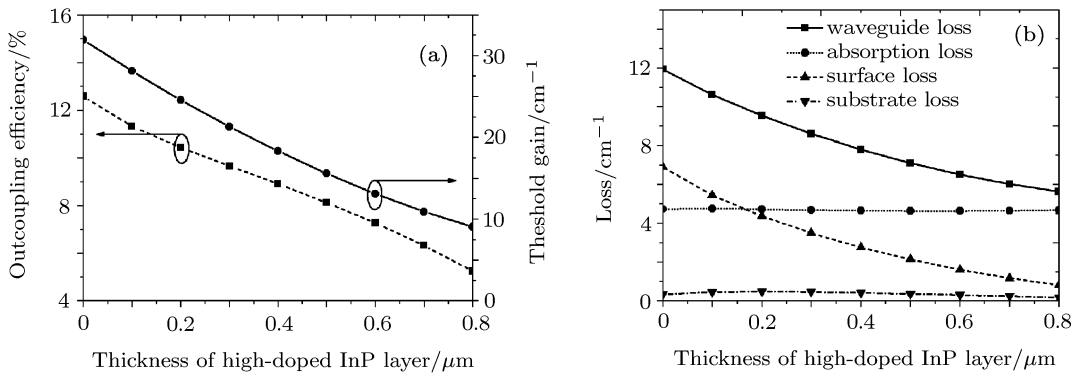


Fig. 2. (a) Surface outcoupling efficiency $\eta_{\rm surf}$ and threshold gain $g_{\rm th}$ versus the thickness of high-doped InP layer, with $|\kappa L| = 1$ used in calculation, and (b) loss coefficients versus the thickness of high-doped InP layer for an infinite length device, with $t_{\rm g} = 1$ μm and $\sigma = 0.6$ used in calculation.

The strong interaction between the radiation field and the surface plasmons pinned at the metal–semiconductor grating interface induces a strong surface loss and a high threshold gain $g_{\rm th}$ as well in a thin-contact-layer-thickness condition. Therefore, a compromise between $\eta_{\rm surf}$ and $g_{\rm th}$ must be taken into consideration in the waveguide design. Given a high outcoupling efficiency that is desired in this work, and a contact layer that is indispensable for providing uniform current injection, a thickness of 0.1 μm for the contact layer is chosen for the convenience of calculations in the rest of this paper. Note that the unoptimized grating parameters used in the calculation may also be responsible for the relatively high threshold gain $g_{\rm th}$ shown in Fig. 2 as discussed below.

3.2. Grating design

The surface outcoupling efficiency $\eta_{\rm surf}$ and the threshold gain $g_{\rm th}$ depend strongly on grating topography. In this section, the grating height $t_{\rm g}$ and due cycle σ are optimized in two steps. According to the wavelength and the waveguide structure the grating period is set to be $\Lambda = 2.41$ μm. Now, first, the behaviours of $g_{\rm th}$ and $\eta_{\rm surf}$, each as a function of $t_{\rm g}$, are investigated as shown in Fig. 3(a), where $\sigma = 0.6$ is used experientially and $|\kappa L| = 1$. Waveguide loss coefficients versus grating height $t_{\rm g}$ are plotted in Fig. 3(b). From these figures, we can find that the substrate loss has an important effect on $\eta_{\rm surf}$ and $g_{\rm th}$, and the absorption loss can be approximated to be a constant within a large range of grating height. The maximum of $\eta_{\rm surf}$ occurs around $t_{\rm g} = 0.8$ μm, where a $(\lambda_n/4)$-effect[14] (λ_n denotes the wavelength travelling in the material) takes place: the air–semiconductor grating layer below the metal-stripe grating acts as an antireflection layer for surface radiation, and hence the surface emission loss is enhanced whereas unwanted radiation loss into the substrate is suppressed effectively. For the shallower or deeper grating, $\eta_{\rm surf}$ decreases because the thickness of air–semiconductor grating layer deviates from the condition of resonance antireflection. The value of $g_{\rm th}$ keeps approximately constant at small $t_{\rm g}$ and has a minimum at $t_{\rm g} = 0.8$ μm, while it increases rapidly from $t_{\rm g} = 1.0$ μm since the radiation loss into the substrate begins to increase abruptly. It is noteworthy that the extreme points of losses and threshold gain appear at different grating heights. This difference mainly results from the finite laser length necessary for the calculation of the threshold gain, but not for that of losses. Consequently, the optimal $t_{\rm g}$ between 0.7–0.9 μm is obtained, and $t_{\rm g} = 0.8$ μm has been used in the following analyses.

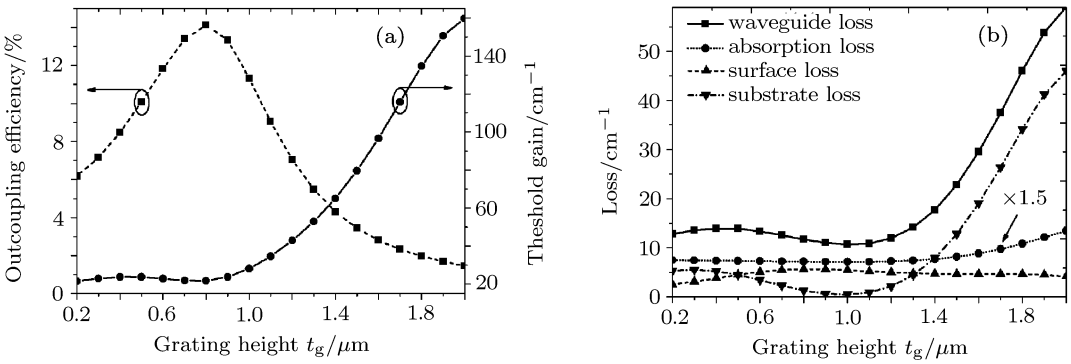


Fig. 3. (a) Surface outcoupling efficiency $\eta_{\rm surf}$ and threshold gain $g_{\rm th}$ versus grating height $t_{\rm g}$, with $|\kappa L| = 1$ used in calculation, and (b) waveguide loss coefficients versus grating height $t_{\rm g}$ for infinite length device, with $\sigma = 0.6$ used in calculation.

Second, the optimization for the duty cycle σ are carried out with $t_{\rm g} = 0.8$ μm by investigating its relations with $\eta_{\rm surf}$, $g_{\rm th}$ and waveguide loss coefficients as shown in Fig. 4. For small duty cycles ($\sigma < 0.3$), a low $\eta_{\rm surf}$ is caused by a small overlap of the optical mode with the grating since a small fraction of metal attracts a small portion of optical field into the grating region. As σ increases, the overlap and hence $\eta_{\rm surf}$ is enhanced untill the value of $\eta_{\rm surf}$ reaches a maximum of 19% at $\sigma = 0.7$. For higher duty cycles ($\sigma > 0.8$), $\eta_{\rm surf}$ decreases because the increasing overlap is jeopardized by the smaller perturbation of the refractive index. Therefore, to achieve a high value of $\eta_{\rm surf}$, the optimal value of σ should be in a range of 0.65–0.75 for the surface emitting second-order

DFB QCL structure. Clearly, $g_{\rm th}$ is affected mainly by the surface loss since the substrate loss is small and the absorption loss varies little. From Fig. 4(b), when σ is less than 0.3, the small perturbation of refractive index results in a small surface loss, and hence low $g_{\rm th}$ is achieved. As σ rises up, surface loss goes up, thereby causing the enhancement of $g_{\rm th}$ which reaches a maximum value at $\sigma = 0.55$. When σ continues to increase, $g_{\rm th}$ begins to come down since total waveguide loss decreases prominently until it achieves a minimum value at $\sigma = 0.75$. For higher duty cycles ($\sigma > 0.8$), $g_{\rm th}$ increases again because absorption loss begins to increase. Consequently, for a lower $g_{\rm th}$ the optimal value of σ should be in a range of 0.7–0.85. From the above analysis, to achieve both high outcoupling efficiency and low threshold gain, σ should be in a range of 0.7–0.75. In our design of device structure, optimal values of $t_{\rm g}$ and σ are set to be about 0.8 μm and 0.7, respectively.

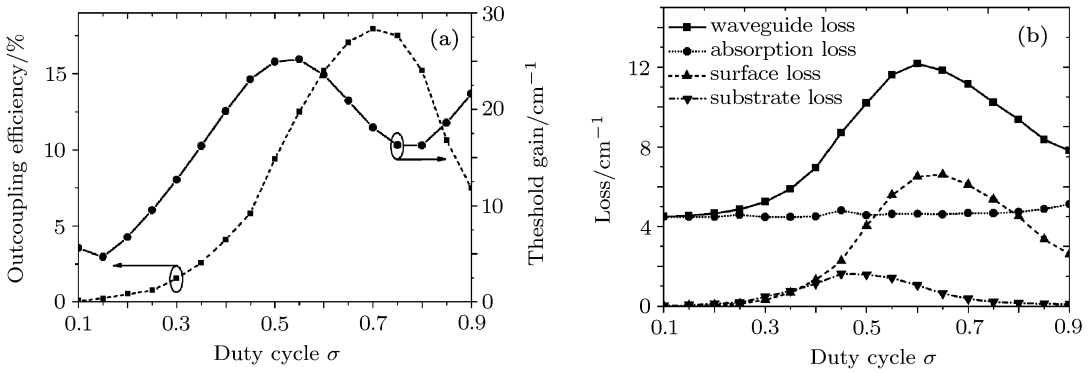


Fig. 4. (a) Surface outcoupling efficiency $\eta_{\rm surf}$ and threshold gain $g_{\rm th}$ versus duty cycle σ, with $|\kappa L| = 1$ used in calculation, and (b) waveguide loss coefficients versus duty cycle σ for an infinite length device with $\sigma = 0.6$ used in calculation.

3.3. Device-length design

For surface emitting second-order DFB QCL structure, the device length L has a strongly influence on the grating coupling strength, thereby affecting the device performance. Figure 5 shows values of $\eta_{\rm surf}$ and $g_{\rm th}$, each as a function of L, with the above optimal results of waveguide and grating designs used in calculation. As the device becomes undercoupling ($|\kappa L| \ll 1$), $g_{\rm th}$ increases rapidly with L decreasing due to facet loss, and $\eta_{\rm surf}$ decreases since the optical intensity is distributed mainly at the ends of the device where only a small portion of power is perpendicularly diffracted into the air. For overcoupling ($|\kappa L| \ll 1$), the value of $g_{\rm th}$ approaches to a constant determined by absorption loss with the increase of L, and $\eta_{\rm surf}$ also comes down because the optical intensity is concentrated in the centre of the device resulting in a very nonuniform power distribution. Whereas, $\eta_{\rm surf}$ displays a very large value of 18%–22% with $|\kappa L| = 1-2$ due to a very uniform power distribution in the device. Therefore, the preferable value of device length is between 2.6–5.4 mm as indicated in the gray area in Fig. 5, while the corresponding $g_{\rm th}$ still maintains a relatively small value between 9 and 18 cm^{-1}. In this paper, a highest surface outcoupling efficiency of 22% with a low threshold gain of 10 cm^{-1} is obtained at an optimal device length of 4.8 mm which is also technologically feasible in the practical device fabrication.

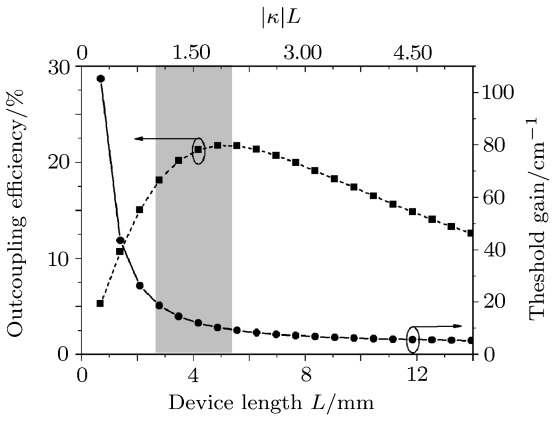


Fig. 5. Surface outcoupling efficiency and threshold gain versus device length L, with $t_{\rm g} = 0.8$ μm and $\sigma = 0.7$ used in calculation.

3.4. Far-field performance

The far-field pattern of surface emission can be expressed as a Fourier transform of the near-field field, given by the following expression[25]

$$\left|\Psi^{\text{farfield}}(\theta)\right|^2 = \cos^2\theta \left| \int_{-\infty}^{\infty} \Phi^{\text{nearfield}}(x) \mathrm{e}^{\mathrm{i}\, kx \sin(\theta)} \right|^2 . \tag{8}$$

For a surface emitting second-order DFB QCL without a grating phaseshift, the lowest threshold mode is antisymmetric, hence the far-field radiation pattern is two-lobed with a null in the centre as depicted in Fig. 6(a). To improve the far field pattern, a π phase shift is introduced by extending a metal tooth in the centre of the grating by $\Lambda/2$[26] and the lasing-mode transforms from antisymmetric to symmetric. Consequently, a single-lobed far field, which is highly desirable for practical applications, is obtained as seen in Fig. 6(b). Note that in our calculations, the π phase shift is included by assuming a sign change for the z-dependent amplitudes, $R(z)$ and $S(z)$.[27]

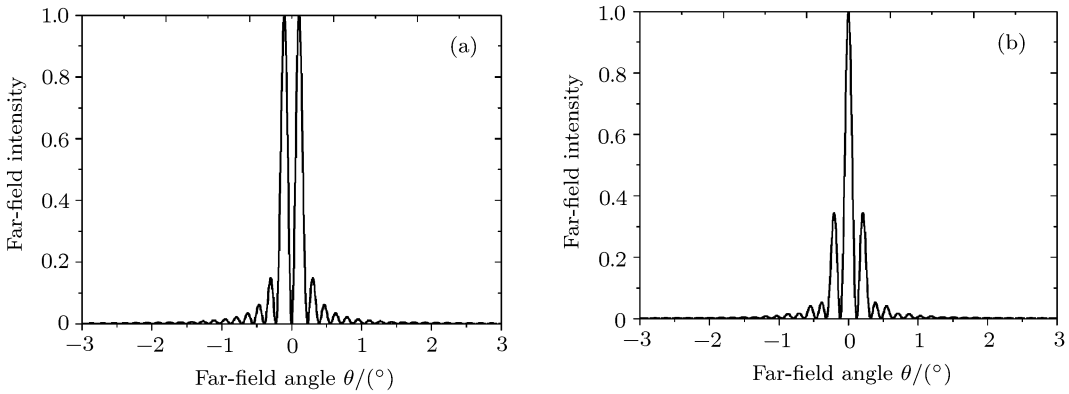


Fig. 6. Far-field patterns of the surface emission for a device without any phase shift (a) and with a π phase shift (b), with $t_{\text{g}} = 0.8$ μm, $\sigma = 0.7$ and $L = 4.8$ mm used in the calculation.

4. Conclusion

We analyse surface emitting second-order DFB QCLs at 7.8 μm based on a coupled-mode theory derived from rigorously computed on-resonant Floquet–Bloch solutions of the waveguide-grating problem. By optimizing the waveguide structure and the grating topography as well as the device length, an optimal surface emitting second-order DFB QCL structure design is proposed, which shows a high surface outcoupling efficiency of 22% and a low threshold gain of 10 cm^{-1}. By adding a π phase-shift in the centre of the grating, a high-quality single-lobe far-field radiation pattern is obtained.

References

[1] Faist J, Capasso F, Sivco D L, Sirtori C, Hutchinson A L and Cho A Y 1994 *Science* **264** 553

[2] Xu G E and Li A Z 2007 *Acta Phys. Sin.* **56** 500 (in Chinese)

[3] Kosterev A A and Tittel F K 2002 *IEEE J. Quantum Electron.* **38** 582

[4] Li H Q, Zhang J, Cui D F, Xu Z Y, Ning Y Q, Yan C L, Qin L, Liu Y, Wang L J and Cao J L 2004 *Acta Phys. Sin.* **53** 2986 (in Chinese)

[5] Hao Y Q, Zhong J C, Ma J L, Zhang Y M and Wang L J 2006 *Chin. Phys.* **15** 1806

[6] Guan B L, Guo X, Yang H, Liang T, Gu X L, Guo J, Deng J, Gao G and Shen G D 2007 *Acta Phys. Sin.* **56** 4585 (in Chinese)

[7] Song G F, Zhang Y, Guo B S and Wang W M 2009 *Acta Phys. Sin.* **58** 7278 (in Chinese)

[8] Hofstetter D, Faist J, Beck M and Oesterle U 1999 *Appl. Phys. Lett.* **75** 3769

[9] Schrenk W, Finger N, Gianordoli S, Hvozdara L, Strasser G and Gornik E 2000 *Appl. Phys. Lett.* **77** 2086

[10] Pflugl C, Austerer M, Schrenk W, Golka S, Strasser G, Green R P, Wilson L R, Cockburn J W, Krysa A B and Roberts J S 2005 *Appl. Phys. Lett.* **86** 211102

[11] Schartner S, Austerer M, Schrenk W, Andrews A M, Klang P and Strasser G 2008 *Opt. Express* **16** 11920

[12] Colombelli R, Srinivasan K, Troccoli M, Painter O, Gmachl C F, Tennant D M, Sergent A M, Sivco D L, Cho A Y and Capasso F 2003 *Science* **302** 1374

[13] Li L 1996 *J. Opt. Soc. Amer.* A **13** 1870

[14] Finger N, Schrenk W and Gornik E 2000 *IEEE J. Quantum Electron.* **36** 780

[15] Finger N and Gornik E 1999 *IEEE J. Quantum Electron.* **35** 832

[16] Streifer W, Burnham R D and Scifres D R 1976 *IEEE J. Quantum Electron.* **QE-12** 737

[17] Noll R J and Macomber S H 1990 *IEEE J. Quantum Electron.* **26** 456

[18] Darvish S R, Zhang W, Evans A, Yu J S, Slivken S and Razeghi M 2006 *Appl. Phys. Lett.* **89** 251119

[19] Wittmann A, Giovannini M, Faist J, Hvozdara L, Blaser S, Hofstetter D and Gini E 2006 *Appl. Phys. Lett.* **89** 141116

[20] Scarpa G, Ulbrich N, Bohm G, Abstreiter G and Amann M C 2003 *IEE Proc. -Optoelecton.* **150** 284

[21] Datta S, Shen S, Roenker K P, Cahay M M and Stanchina W E 1998 *IEEE Trans. Electron Devices* **45** 1634

[22] Shokhovets S, Ambacher O and Gobsch G 2007 *Phys. Rev.* B **76** 125203

[23] Levinshtein M, Rumyantsev S and Shur M 1996 *Handbook Series on Semiconductor Parameters* (Vol. 1) (Singapore: World Scientific) p169

[24] Bahriz M, Moreau V, Palomo J, Colombelli R, Austin D A, Cockburn J W, Wilson L R, Krysa A B and Roberts J S 2006 *Appl. Phys. Lett.* **88** 181103

[25] Agrawal G P and Dutta N K 1986 *Long-wavelength Semiconductor Lasers* (New York: van Nostrand) p61

[26] Li S, Witjaksono G, Macomber S and Botez D 2003 *IEEE J. Sel. Top. Quantum Electron.* **9** 1153

[27] Schubert M and Rana F 2006 *IEEE J. Quantum Electron.* **42** 257